Effect of the Polydispersity of a Colloidal Drop on Drying Induced Stress as Measured by the Buckling of a Floating Sheet

François Boulogne, Yong Lin Kong, Janine K. Nunes, and Howard A. Stone
Department of Mechanical and Aerospace Engineering, Princeton University, Princeton, New Jersey 08544, USA
(Received 19 February 2016; published 8 June 2016)

We study the stress developed during the drying of a colloidal drop of silica nanoparticles. In particular, we use the wrinkling instability of a thin floating sheet to measure the net stress applied by the deposit on the substrate and we focus on the effect of the particle polydispersity. In the case of a bidisperse suspension, we show that a small number of large particles substantially decreases the expected stress, which we interpret as the formation of lower hydrodynamic resistance paths in the porous material. As colloidal suspensions are usually polydisperse, we show for different average particle sizes that the stress is effectively dominated by the larger particles of the distribution and not by the average particle size.

DOI: 10.1103/PhysRevLett.116.238001

Drying of colloidal droplets is ubiquitous in processes such as ink-jet printing technologies [1] or spray painting. Recently, new directions for printing techniques have been developed for soft materials to enable applications such as conformable electronics, soft robotics, and wearable devices. For instance, electronic circuits can be printed on elastomers [2,3] and human skin [4]. However, deformations of the surface can be induced by the surface tension of a liquid drop [5–7] or the consolidation of a colloidal material [8], which could affect the final quality and the function of the printed device. Here, we report measurements of the drying induced stress and highlight the role of polydispersity of the suspension.

Previous reported measurements of drying or cracking stresses rely on the deflection of a cantilever beam [9–12], where a liquid film of a polymer solution or colloidal suspension is coated on a thin flexible plate. In such a geometry, the film dries from the edge toward the center of the film [13], which leads to spatially inhomogeneous states of the material.

However, besides the bending, when a stress is applied above a certain limit to a thin sheet, a wrinkling instability can be observed [14–17]. Recent studies focused on an elastomeric disk floating on a liquid bath with a liquid drop in the center of the disk [18–22]. In these situations, the stress applied to the membrane is due to the surface tension of the involved liquids. Therefore, these studies of a deformable sheet established models based on Föppl–von Kàrmàn equations to predict the length and the number of wrinkles.

In this Letter, we focus on visualizing and measuring the stress induced by the drying of a colloidal drop on a floating membrane (Fig. 1). The mechanical properties of the membrane are chosen carefully to satisfy two conditions. First, the surface tension of the pure liquid drop alone and its weight do not trigger the wrinkling instability [Fig. 1(a)]. Second, the drying-induced consolidation of the colloidal droplet, which induces a larger tensile stress in the membrane, triggers the instability [Fig. 1(b)]. From the length of the wrinkles, we can deduce the tension in the film. Our aim is to examine the effect of particle size and polydispersity on the net stress that a drying drop of silica nanoparticles applies on the substrate.

Elastomeric sheets are prepared with polydimethylsiloxane (PDMS) by a spin coating technique on a silicon wafer (see Sec. S1 in the Supplemental Material [23]). The measured film thickness ranges from $[15.8, 63.9]$ μm, the elastic modulus of the floating film is $E_s = 1.2$ MPa and the Poisson ratio $\nu = 0.5$. Thus, the bending modulus $\mathcal{B} = [E_s h^3/12(1-\nu^2)]$ of the thin sheet is $\mathcal{B} \in [5.3, 350] \times 10^{-10}$ Pa m^3. The floating film is detached from the wafer in a water bath, which has a surface tension $\gamma_b = 55 \pm 5$ mN/m.

The colloidal suspensions are silica nanoparticles. SM, HS, and TM are Ludox suspensions (purchased from Sigma-Aldrich), and Kleb and Lev denote Klebosol 50R50 and Levasil30, respectively (Table S1, in the Supplemental

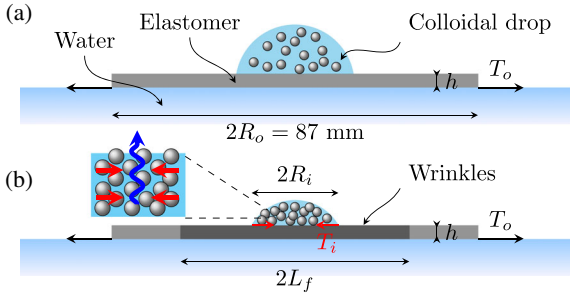

FIG. 1. Schematic of the experimental set up. A thin elastomeric sheet floats on a water bath. (a) The initial state where no wrinkles are observed after the drop deposition. (b) The final consolidated state where wrinkles extend over a total length $2L_f$. The picture illustrates the drying stress induced by the Darcy flow in the porous material.

Material [23]). To ensure that all suspensions have the same pH, ionic strength, and volume fraction, each suspension is dialyzed [25] and has an initial volume fraction $\phi_0 = 0.15$. The particle size distributions are characterized by dynamic light scattering (DLS) and the average particle diameters $2a_0$ span from 7 to 92 nm. Details on the sample preparation and on the particle size characterization are presented in Sec. S2 in the Supplemental Material [23]. A drop of colloidal suspension of 8 $\mu\ell$ is dispensed with a micropipette in the center of the floating sheet (Fig. 1). Pictures of the floating film are recorded in a humidity controlled chamber ($R_H = 50\%$) every minute.

Initially, no wrinkles are present on the floating film. As the colloidal drop dries, the contact line first exhibits a stick-slip motion. Ultimately, the contact line pins, the deposit height decreases and, concurrently, the wrinkling instability appears at $t_i = 110 \pm 15$ min [Fig. 2(a)]. The length of the wrinkled region grows linearly in time until it reaches a final length L_f when the colloidal drop becomes solid at $t_f = 150 \pm 15$ min [Fig. 2(b)]. During the consolidation, no relaxation of the wrinkles is observed, which indicates that the deposit is in good adhesion with the substrate (Fig. 2). This observation is supported by a side view showing that the contact line is pinned during the development of the wrinkling instability and the drop height decreases (see movie in the Supplemental Material [23]). Furthermore, no cracks are visible in the final colloidal deposit, which is due to the substrate elasticity [26].

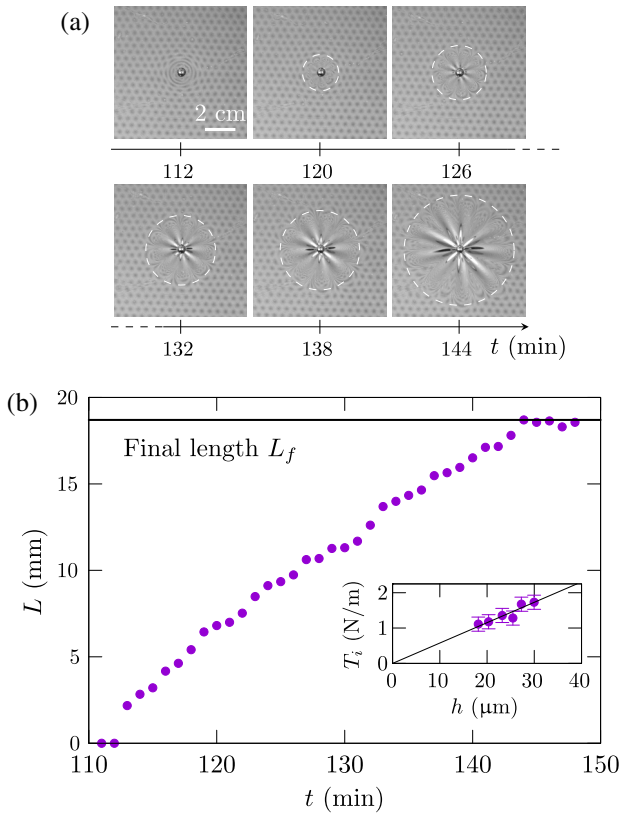

FIG. 2. (a) Illustration of the expansion of wrinkles for a 8 $\mu\ell$ drop of SM particles on a film of thickness $h = 20$ μm. (b) The main plot shows the time evolution of the length $L(t)$ measured on the pictures shown above. The inset represents the inner tension T_i deduced from Eq. (2) for different film thicknesses h and for TM particles.

To obtain an estimate of the time evolution of the volume fraction, the time derivative of the liquid volume is $dV(t)/dt = -j$ where j is the evaporative flux [27]. To estimate this flux, we consider that the aggregation occurs at $\phi_f = \phi(t_f) \approx 0.6$ [28]. Thus, we have $j \approx V_0(1-\phi_0)/t_f$ and $V(t) \approx (1-\phi_0)V_0 - jt$. Therefore, the evaporation speed scales as $v_e \sim j/S \approx 1 \times 10^{-7}$ m/s, where $S \approx 2\pi R_i^2$ is the characteristic evaporating area. The instability appears for $\phi(t_i) \approx 0.37$, which is the typical volume fraction for which the material becomes viscoplastic [28,29].

As we observed, the growth of the wrinkle length is associated with the consolidation of the deposit, which applies a tensile stress on the membrane. We employ the final length of wrinkles to quantify this stress. Davidovitch *et al.* predicted the wrinkle's length as a function of the inner tension T_i applied by the deposit at $r = R_i$ and the outer tension $T_o = \gamma_b$ due to the surface tension of the liquid bath at $r = R_o$ (Fig. 1) [19]. The wrinkles morphology is set by the tension ratio $\tau = T_i/T_o$ and the bendability $\epsilon^{-1} = R_i^2 T_o/\mathcal{B}$. With a stability analysis of the Föppl–von Kàrmàn equations for $\epsilon \ll 1$, the length of the wrinkles is predicted to be

$$L_{\mathrm{NT}} = R_i\sqrt{T_i/T_o - 1}. \tag{1}$$

This relation is valid for infinitesimal deformation amplitudes ζ and is called the near threshold limit (NT).

A second limit was also established for finite deformation amplitudes ζ. For $\epsilon \to 0$, Davidovitch *et al.* assume that in the postbuckling region, the hoop stress $\sigma_{\theta\theta}$ and the shear stress $\sigma_{r\theta}$ vanish. In this far from threshold limit (FFT), the wrinkle length is predicted to be

$$L_{\mathrm{FFT}} = \frac{R_i T_i}{2T_o}. \tag{2}$$

In our experimental conditions, the total number of wrinkles is established early in the development of the wrinkles as previously observed in wetting experiments [21]. Also, this number varies weakly, typically between 6 and 12, as the physical parameters are changed, which does not allow a prediction from this quantity described by scaling laws in the literature [19–21]. From the final length of wrinkles L_f, the inner tension can be estimated in NT and FFT limits from Eqs. (1) and (2), respectively. In our experimental conditions, the T_i^{NT} values are about an order of magnitude above the range of NT tension values predicted by Davidovitch *et al.* [19] (Sec. S4, Supplemental

Material [23]). Consequently, inner tension values are calculated in the FFT limit from Eq. (2).

We performed experiments with a TM suspension, a drop volume of 8 $\mu\ell$, and different film thicknesses. The tension T_i resulting from the final wrinkle length [Eq. (2)] is plotted as a function of the film thickness h in the inset of Fig. 2(b). The linear relationship between T_i and h suggests that the relevant parameter to describe the consolidation of the deposit on the membrane is the average stress $\sigma_i = T_i/h$.

Since the deposit has a good adhesion on the elastomer [8], the drying strain in the deposit is transmitted to the flexible membrane, which leads to the formation of wrinkles. In the following, we consider that the deposit generates an effective stress σ_i in the membrane located at the deposit edge.

To study the effect of the particle size polydispersity [30,31] on the drying stress, we prepared blended suspensions from SM and Lev samples (Table S1). Since Lev particles are larger than the largest particles present in the SM suspension, we consider as a first approximation that the mixture is a bidisperse suspension; the size ratio is approximately a factor of 10. We denote a_s and a_ℓ, the average radii of small and large particles, respectively. The volume ratio of large particles is defined as

$$\Gamma_\mathcal{V} = \frac{\mathcal{V}_\ell}{\mathcal{V}_s + \mathcal{V}_\ell}, \tag{3}$$

where $\mathcal{V}$ is the volume of particles. Equivalently, denoting $\mathcal{N}_s$ and $\mathcal{N}_\ell$ as the number of small and large particles, we define the particle number ratio of large particles as

$$\Gamma_\mathcal{N} = \frac{\mathcal{N}_\ell}{\mathcal{N}_s + \mathcal{N}_\ell} = \left[1 + \frac{a_\ell^3}{a_s^3}(\Gamma_\mathcal{V}^{-1} - 1)\right]^{-1}. \tag{4}$$

We conducted a first set of experiments that consist in drying drops of colloids on a hydrophilic glass slide. The drying occurs from the contact line toward the center as the edge is thinner and the evaporative flux is highest at the edge. During the consolidation, the material delaminates from the substrate and the curvature increases with the tensile stress [32]. In Fig. 3(a), we observe that the addition of a small number of large particles reduces significantly the delamination, which could be crucial for coating applications. Next, we investigate the stress reduction caused by the presence of these large particles.

Since measurements of the drying stress are possible with the floating film (Fig. 2), we quantify the effect of the particle size ratio. As the evaporation may lead to particle segregation in the deposit [33–35], we checked the particle organization across the thickness of the deposit by SEM. We observed that the particles remains homogeneously distributed at the end of the drying [Fig. 3(b) and Supplemental Material, Sec. S3 [23]].

Our experiments showed that the length of the wrinkles decreases as the number fraction of large particles increases

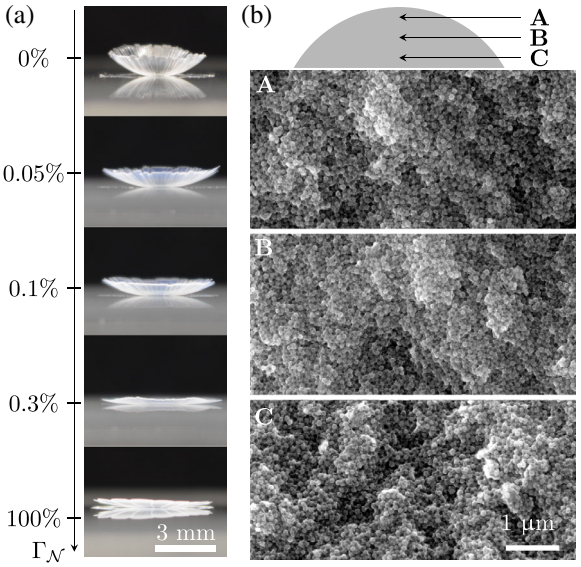

FIG. 3. (a) Delamination of colloidal drops upon drying on a glass slide for different number ratios $\Gamma_\mathcal{N}$. Pictures are taken at the maximum elevation. The initial volume is 6 $\mu\ell$ and the initial volume fraction of the suspensions is 0.15. (b) Scanning-electron-microscope (SEM) images in the cross section of a dried deposit at a number ratio $\Gamma_\mathcal{N} = 0.003$. Positions are indicated by the schematic.

[Fig. 4(a)]. The stress $\sigma_i = T_i^{\mathrm{FFT}}/h = 2T_o L_{\mathrm{FFT}}/(R_i h)$ after drying is reported in Fig. 4(b) as a function of $\Gamma_\mathcal{N}$ and $\Gamma_\mathcal{V}$. First, we find that the drying stress for a pure suspension of large particles ($\Gamma_\mathcal{N} = 1$) is about half as large as the case of a pure suspension of small particles ($\Gamma_\mathcal{N} = 0$), which confirms that the final stress depends on the particle size. These results also show that the addition of a number density $\Gamma_\mathcal{N} \approx 0.003$ of large particles ($\Gamma_\mathcal{V} \approx 0.7$) leads to a stress value comparable to a suspension of only large particles.

To interpret these results, we refer to the description developed by Sherwood [36] and further detailed in particular by Brinker and Scherer [37]. During the drying of the colloidal suspension, the particles concentrate and form a porous material for which the surface remains wet. The liquid flow driven by the evaporation generates a pressure gradient due to the Darcy law, which is responsible for a tensile stress in the deposit [37,38]. When the compression exceeds the repulsive interactions between the colloids, silica particles irreversibly aggregate [30] and the menisci penetrate in the material [39].

We use the Darcy approximation $\eta \boldsymbol{v}/k(a) = -\boldsymbol{\nabla} p$, where $\eta = 10^{-3}$ Pa s is the solvent viscosity, $\boldsymbol{v}$ is the fluid velocity, p is the pressure and $k(a)$ is the permeability. We can estimate the tensile stress σ_d from the pressure gradient in the porous network as

$$\sigma_d \sim \frac{R_i \eta v_e}{k(a)}, \tag{5}$$

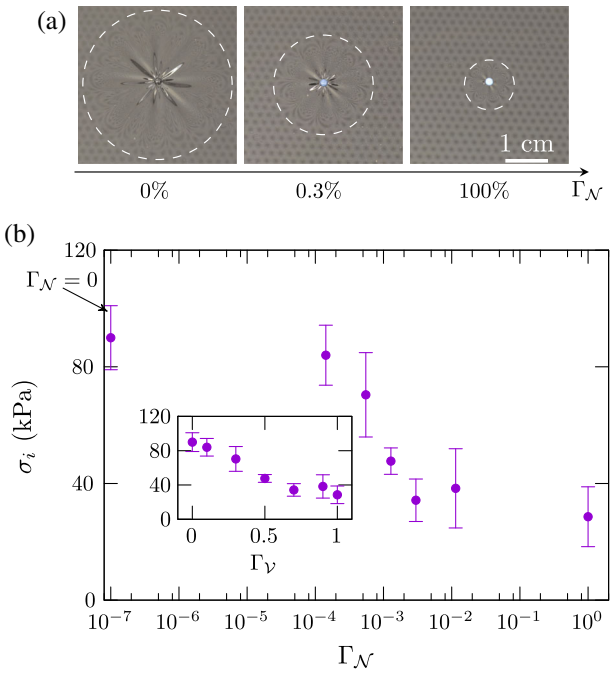

FIG. 4. (a) Pictures of the final state for three different number ratios $\Gamma_\mathcal{N}$ [Eq. (4)]. (b) Final tensile stress σ_i applied by a deposit on a membrane for a bidisperse suspension indicated by the number ratio of large particles $\Gamma_\mathcal{N}$. The inset shows the same data as a function of $\Gamma_\mathcal{V}$ [Eq. (3)].

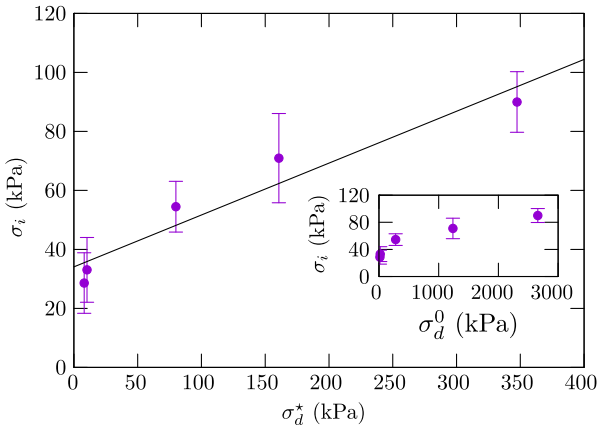

FIG. 5. Stress $\sigma_i = T_i/h$ as a function of the Darcy stress σ_d [Eq. (5)]. In the main plot, $\sigma_d^\star$ is calculated for the permeability $k(a^\star)$ where the particle radius $a^\star$ is representative of the large particles size of the distribution. The inset shows the same results for σ_d^0 related the average particle size a_0. The solid line is a guide for the eye.

where R_i is the deposit size, and v_e is the evaporation speed. For a characteristic particle size $a = 25$ nm and $R_i = 0.8$ mm, we have $\sigma_d \approx 30$ kPa, which is comparable to the measured σ_i. For a monodisperse suspension of particle radius a, the permeability depends on the square of the pore size and can be calculated by the Carman-Kozeny relation $k(a) = [a^2(1-\phi_f)^3/45\phi_f^2]$, where ϕ_f is the final volume fraction. We observed that the large particles dominate the stress even if they are present at a low number fraction [Fig. 4(b)]. We interpret this observation as indicating the formation of a continuous path for flow due to large pore sizes formed by the large particles, which increases the permeability.

We performed experiments for different average particle sizes. The results are represented in Fig. 5 and the inset shows the stress σ_i calculated from the wrinkle length as a function of the Darcy stress σ_d^0 for the average particle size a_0 [Eq. (5)]. For the permeability, the Carman-Kozeny relation is used to calculate a characteristic value. Moreover, we define a particle size $a^\star$ to take into account the particle polydispersity. This size is defined as the average particle size of the 30% largest particles of the distribution (Sec. S2, Supplemental Material [23]). From these values, we calculate the Darcy stress $\sigma_d^\star$ shown in Fig. 5. These results indicate that the stress measured from the length of the wrinkles is comparable to $\sigma_d^\star$, while it is significantly different if the average particle size is considered. Thus, we conclude that the large particles plays a major role in the final drying stress of a colloidal suspension. The detailed relationship between the drying stress and the stress in the membrane remains to be established and has to account for the geometrical aspects of the deposit and the deformation of the membrane beneath the deposit.

In summary, we have studied the consolidation of colloidal silica nanoparticles in the geometry of a drop placed in the center of a thin circular elastomeric sheet floating on a liquid bath. As the drying proceeds, the consolidation of the colloidal drop triggers a wrinkling instability of the membrane. We demonstrated that this technique allows a measurement of the final tensile stress applied by the deposit on the substrate. We used this method to measure the effects of the particle size and the polydispersity.

For a mixture of small and large particles with a typical size ratio of about 10, the addition of about 1% of large particles reduces the stress value obtained for the suspension of small particles to the value observed for large particles only. Indeed, colloidal suspensions are generally polydisperse. Our work provides evidence that the contribution of the particle size polydispersity on the tensile stress is dominated by the largest particles. We interpreted these results by the percolation of the largest particles that creates paths with a larger pore size, which reduces the tensile stress due to the pressure gradient of the Darcy flow, accompanying evaporation of the liquid.

We believe that these results are significant for future investigations regarding the quantitative measurement of the drying stress in more complex materials. Our findings could influence the study of the emergence of tensile stress in drying materials, which often leads to delamination or substrate deformations that must be avoided in many technological applications. As future work, it will be

important to derive a numerical or theoretical model to understand more quantitatively the effect of the polydispersity on the tensile stress.

We are very grateful to I. Cantat, B. Davidovitch, B. Saintyves, and J.-B. Salmon for stimulating discussions. We thank J.-M. Copin and M. Persson for providing Klebosol and Levasil samples, respectively. We also thank R. K. Prud'homme for the use of the Malvern Zetasizer, J. Feng and B. K. Wilson for assistance, as well as J. Schreiber for assistance with SEM images. F. B. acknowledges that the research leading to these results received funding from the People Programme (Marie Curie Actions) of the European Union's Seventh Framework Programme (FP7/2007-2013) under REA Grant Agreement No. 623541.

[1] D. James, B. K. C Kjellander, W. T. Smaal, G. Gelinck, C. Combe, I. McCulloch, R. Wilson, J. Burroughes, D. C. Bradley, and J.-S. Kim, Thin-film morphology of inkjet-printed single-droplet organic transistors using polarized Raman spectroscopy: effect of blending TIPS-pentacene with insulating polymer, ACS Nano **5**, 9824 (2011).

[2] J. A. Rogers, T. Someya, and Y. Huang, Materials and mechanics for stretchable electronics, Science **327**, 1603 (2010).

[3] J. Boley, E. White, and R. Kramer, Mechanically sintered gallium-indium nanoparticles, Adv. Mater. **27**, 2355 (2015).

[4] J.-W. Jeong, W.-H. Yeo, A. Akhtar, J. S. Norton, Y.-J. Kwack, S. Li, S.-Y. Jung, Y. Su, W. Lee, J. Xia, H. Cheng, Y. Huang, W.-S. Choi, T. Bretl, and J. Rogers, Materials and optimized designs for human-machine interfaces via epidermal electronics, Adv. Mater. **25**, 6839 (2013).

[5] E. Jerison, Y. Xu, L. A. Wilen, and E. R. Dufresne, Deformation of an Elastic Substrate by A Three-Phase Contact Line, Phys. Rev. Lett. **106**, 186103 (2011).

[6] A. Marchand, S. Das, J. Snoeijer, and B. Andreotti, Contact angles on a soft solid: from Young's law to Neumann's law, Phys. Rev. Lett. **109**, 236101 (2012).

[7] J. Dervaux and L. Limat, Contact lines on soft solids with uniform surface tension: Analytical solutions and double transition for increasing deformability, Proc. R. Soc. A **471**, 1 (2015).

[8] F. Boulogne and H. A. Stone, Self-crumpling elastomers: bending induced by the drying stimulus of a nanoparticle suspension, Europhys. Lett. **108**, 19001 (2014).

[9] C. Petersen, C. Heldmann, and D. Johannsmann, Internal stresses during film formation of polymer latices, Langmuir **15**, 7745 (1999).

[10] H. N. Yow, M. Goikoetxea, L. Goehring, and A. F. Routh, Effect of film thickness and particle size on cracking stresses in drying latex films, J. Colloid Interface Sci. **352**, 542 (2010).

[11] K. R. Thomas and U. Steiner, Direct stress measurements in thin polymer films, Soft Matter **7**, 7839 (2011).

[12] M. Chekchaki and V. Lazarus, Mechanical stresses induced by evaporation in consolidated colloidal suspensions of hard particles. poroelasticity theory versus experiments, Transp. Porous Media **100**, 143 (2013).

[13] J. Li, B. Cabane, M. Sztucki, J. Gummel, and L. Goehring, Drying dip-coated colloidal films, Langmuir **28**, 208 (2012).

[14] E. Cerda and L. Mahadevan, Geometry and physics of wrinkling, Phys. Rev. Lett. **90**, 074302 (2003).

[15] J.-C. Géminard, R. Bernal, and F. Melo, Wrinkle formations in axi-symmetrically stretched membranes, Eur. Phys. J. E **15**, 117 (2004).

[16] O. Oshri, F. Brau, and H. Diamant, Wrinkles and folds in a fluid-supported sheet of finite size, Phys. Rev. E **91**, 052408 (2015).

[17] P. Damman, *Polymer Surfaces in Motion: Unconventional Patterning Methods* (Springer International Publishing, New York, 2015), Chap. 8, p. 183.

[18] J. Huang, M. Juszkiewicz, W. De Jeu, E. Cerda, T. Emrick, N. Menon, and T. Russell, Capillary wrinkling of floating thin polymer films, Science **317**, 650 (2007).

[19] B. Davidovitch, R. Schroll, D. Vella, M. Adda-Bedia, and E. Cerda, Prototypical model for tensional wrinkling in thin sheets, Proc. Natl. Acad. Sci. U.S.A. **108**, 18227 (2011).

[20] H. King, R. Schroll, B. Davidovitch, and N. Menon, Elastic sheet on a liquid drop reveals wrinkling and crumpling as distinct symmetry-breaking instabilities, Proc. Natl. Acad. Sci. U.S.A. **109**, 9716 (2012).

[21] K. B. Toga, J. Huang, K. Cunningham, T. P. Russell, and N. Menon, A drop on a floating sheet: boundary conditions, topography and formation of wrinkles, Soft Matter **9**, 8289 (2013).

[22] M. Pineirua, N. Tanaka, B. Roman, and J. Bico, Capillary buckling of a floating annulus, Soft Matter **9**, 10985 (2013).

[23] See Supplemental Material http://link.aps.org/supplemental/10.1103/PhysRevLett.116.238001 for [brief description], which includes Refs. [19–24].

[24] M. Taylor, B. Davidovitch, Z. Qiu, and K. Bertoldi, A comparative analysis of numerical approaches to the mechanics of elastic sheets, J. Mech. Phys. Solids **79**, 92 (2015).

[25] A. Bouchoux, P.-E. Cayemitte, J. Jardin, G. Gésan-Guiziou, and B. Cabane, Casein micelle dispersions under osmotic stress, Biophys. J. **96**, 693 (2009).

[26] M. I. Smith and J. S. Sharp, Effects of substrate constraint on crack pattern formation in thin films of colloidal polystyrene particles, Langmuir **27**, 8009 (2011).

[27] R. Deegan, O. Bakajin, T. Dupont, G. Huber, S. Nagel, and T. Witten, Contact line deposits in an evaporating drop, Phys. Rev. E **62**, 756 (2000).

[28] F. Boulogne, L. Pauchard, F. Giorgiutti-Dauphiné, R. Botet, R. Schweins, M. Sztucki, J. Li, B. Cabane, and L. Goehring, Structural anisotropy of directionally dried colloids, Europhys. Lett. **105**, 38005 (2014).

[29] E. Di Giuseppe, A. Davaille, E. Mittelstaet, and M. Francois, Rheological and mechanical properties of silica colloids: from Newtonian liquid to brittle behaviour, Rheol. Acta **51**, 451 (2012).

[30] R. Iler, *The Chemistry of Silica: Solubility, Polymerization, Colloid and Surface Properties and Biochemistry of Silica* (Wiley-Interscience, New York, 1979).

[31] P. Lidon and J.-B. Salmon, Dynamics of unidirectional drying of colloidal dispersions, Soft Matter **10**, 4151 (2014).

[32] L. Pauchard, Patterns caused by buckle-driven delamination in desiccated colloidal gels, Europhys. Lett. **74**, 188 (2006).
[33] R. E. Trueman, E. Lago Domingues, S. N. Emmett, M. W. Murray, J. L. Keddie, and A. F. Routh, Autostratification in drying colloidal dispersions: experimental investigations, Langmuir **28**, 3420 (2012).
[34] A. F. Routh, Drying of thin colloidal films, Rep. Prog. Phys. **76**, 046603 (2013).
[35] A. Fortini, I. Martín-Fabiani, J. L. De La Haye, P.-Y. Dugas, M. Lansalot, F. D'Agosto, E. Bourgeat-Lami, J. L. Keddie, and R. P. Sear, Dynamic Stratification in Drying Films of Colloidal Mixtures, Phys. Rev. Lett. **116**, 118301 (2016).
[36] T. K. Sherwood, The drying of solids I, Ind. Eng. Chem. **21**, 12 (1929).
[37] C. J. Brinker and G. W. Scherer, *Sol-Gel Science: The Physics and Chemistry of Sol-Gel Processing* (Academic Press, New York, 1990).
[38] F. Boulogne, F. Giorgiutti-Dauphiné, and L. Pauchard, Surface patterns in drying films of silica colloidal dispersions, Soft Matter **11**, 102 (2015).
[39] J. Thiery, S. Rodts, E. Keita, X. Chateau, P. Faure, D. Courtier-Murias, T. E. Kodger, and P. Coussot, Water transfer and crack regimes in nanocolloidal gels, Phys. Rev. E **91**, 042407 (2015).